MANCHESTER
1824
The University of Manchester

The University of Manchester Research

IL-1R8 is a checkpoint in NK cells regulating anti-tumour and anti-viral activity

DOI:
10.1038/nature24293

Document Version
Accepted author manuscript

Link to publication record in Manchester Research Explorer

Citation for published version (APA):
Molgora, M., Bonavita, E., Ponzetta, A., Riva, F., Barbagallo, M., Jaillon, S., Popovi, B., Bernardini, G., Magrini, E., Gianni, F., Zelenay, S., Jonji, S., Santoni, A., Garlanda, C., & Mantovani, A. (2017). IL-1R8 is a checkpoint in NK cells regulating anti-tumour and anti-viral activity. *Nature*, *551*(7678), 110-114. https://doi.org/10.1038/nature24293

Published in:
Nature

Citing this paper
Please note that where the full-text provided on Manchester Research Explorer is the Author Accepted Manuscript or Proof version this may differ from the final Published version. If citing, it is advised that you check and use the publisher's definitive version.

General rights
Copyright and moral rights for the publications made accessible in the Research Explorer are retained by the authors and/or other copyright owners and it is a condition of accessing publications that users recognise and abide by the legal requirements associated with these rights.

Takedown policy
If you believe that this document breaches copyright please refer to the University of Manchester's Takedown Procedures [http://man.ac.uk/04Y6Bo] or contact uml.scholarlycommunications@manchester.ac.uk providing relevant details, so we can investigate your claim.

Download date:26. Aug. 2022

IL-1R8 is a checkpoint in NK cells regulating anti-tumor and anti-viral activity

Martina Molgora[1,*], Eduardo Bonavita[1,*,°], Andrea Ponzetta[1], Federica Riva[2], Marialuisa Barbagallo[1], Sébastien Jaillon[1,3], Branka Popović[4], Giovanni Bernardini[5], Elena Magrini[1], Francesca Gianni[1], Santiago Zelenay[6], Stipan Jonjić[4], Angela Santoni[5], Cecilia Garlanda[1,a], Alberto Mantovani[1,3,7,a]

[1]Humanitas Clinical and Research Center, Rozzano, Italy

[2]Department of Animal Pathology, Faculty of Veterinary Medicine, University of Milan, Italy

[3]Humanitas University, 20089 Rozzano, Italy

[4]Faculty of Medicine, University of Rijeka, 51000 Rijeka, Croatia

[5]Dipartimento di Medicina Molecolare Istituto Pasteur-Fondazione Cenci Bolognetti, Università di Roma "La Sapienza" 00161 Rome, Italy

[6] Cancer Research UK Manchester Institute, The University of Manchester, Manchester, M20 4QL, United Kingdom

[7] The William Harvey Research Institute, Queen Mary University of London, London, EC1M 6BQ, United Kingdom

* MM and EB contributed equally to this work.

° Present address: Cancer Research UK Manchester Institute, The University of Manchester, Manchester, M20 4QL, United Kingdom

Running title: IL-1R8 is a checkpoint molecule of NK cells

[a] Corresponding authors:

Alberto Mantovani, MD
Humanitas Clinical and Research Center
Via Manzoni 56, 20089 Rozzano, Italy
alberto.mantovani@humanitasresearch.it

or Cecilia Garlanda

28 Humanitas Clinical and Research Center
29 Via Manzoni 56, 20089 Rozzano, Italy
30 cecilia.garlanda@humanitasresearch.it

Interleukin-1 receptor 8 (IL-1R8, also known as single immunoglobulin IL-1R-related receptor, SIGIRR, or TIR8) is a member of the IL-1 receptor (ILR) family with distinct structural and functional characteristics, acting as a negative regulator of ILR and Toll-like receptor (TLR) downstream signaling pathways and inflammation[1]. NK cells are innate lymphoid cells which mediate resistance against pathogens and contribute to the activation and orientation of adaptive immune responses[2-4]. NK cells mediate resistance against hematopoietic neoplasms but are generally considered to play a minor role in solid tumor carcinogenesis[5-7]. Here we report that IL-1R8 serves as a checkpoint for NK cell maturation and effector function. Its genetic blockade unleashes NK-cell mediated resistance to hepatic carcinogenesis, hematogenous liver and lung metastasis and cytomegalovirus infection.

Several lines of evidence suggest that IL-1R8 interferes with the association of TIR module-containing adaptor molecules with signaling receptor complexes of the ILR or TLR family, tuning downstream signaling, thus negatively controlling inflammatory and immune responses and T helper (TH) cell polarization and functions[1,8]. Moreover, IL-1R8 is the co-receptor of IL-1R5/IL-18Rα for IL-37, and is required for the anti-inflammatory activity of this human cytokine[9]. Deregulated activation by ILR or TLR ligands in IL-1R8-deficient mice has been associated with exacerbated inflammation and immunopathology, including selected cancers, or autoimmune diseases[10].

IL-1R8 is widely expressed[10]. However, we found strikingly high levels of IL-1R8 mRNA and protein in human NK cells, compared to other circulating leukocytes and monocyte-derived macrophages (Fig. 1a, Extended Data Fig. 1a). *IL1R8* mRNA levels increased during NK cell maturation[11] (Extended Data Fig. 1b) and surface protein expression mirrored transcript levels (Fig. 1b, Extended Data Fig. 1c). IL-1R8 expression was detected at low level in bone marrow pluripotent haematopoietic stem cells and NK cell precursors and was selectively upregulated in mature NK cells and not in $CD3^+$ lymphocytes (Extended Data Fig. 1d).

56 Murine NK cells expressed significantly higher levels of *Il1r8* mRNA, compared to other
57 leukocytes (Fig. 1c) and relative to other ILRs (Extended Data Fig. 1e, 1f). In line with the results
58 obtained in human NK cells, *Il1r8* mRNA level increased during the 4-stage developmental
59 transition from $CD11b^{low}CD27^{low}$ to $CD11b^{high}CD27^{low}$[12] (Fig. 1d, Extended Data Fig. 1g).

60 To assess the role of IL-1R8 in NK cells, we took advantage of IL-1R8-deficient mice.
61 Among $CD45^{+}$ cells, the NK cell frequency and absolute numbers were significantly higher in
62 peripheral blood of *Il1r8*$^{-/-}$ compared to *Il1r8*$^{+/+}$ mice and slightly increased in liver and spleen.
63 (Fig. 2a, 2b). In addition, the frequency of the $CD11b^{high}CD27^{low}$ and $KLRG1^{+}$ mature subset was
64 significantly higher in *Il1r8*$^{-/-}$ mice compared to *Il1r8*$^{+/+}$ mice in BM, spleen and blood, indicating a
65 more mature phenotype of NK cells[13] (Fig. 2c, 2d, Extended Data Fig. 2a, 2b).

66 The enhanced NK cell maturation in *Il1r8*$^{-/-}$ mice occurred already at 2 and 3 weeks of age,
67 whereas the frequency of NK precursors was similar in *Il1r8*$^{-/-}$ and *Il1r8*$^{+/+}$ BM, indicating that IL-
68 1R8 regulated early events in NK cell differentiation, but did not affect the development of NK cell
69 precursors (Extended Data Fig. 2c-e)[12].

70 We next investigated whether IL-1R8 impacted on NK cell function. The expression of the
71 activating receptors NKG2D, DNAM-1 and Ly49H was significantly upregulated in peripheral
72 blood *Il1r8*$^{-/-}$ NK cells (Extended Data Fig. 2f). IFNγ and Granzyme B production and FasL
73 expression were more sustained in IL-1R8-deficient NK cells upon ex-vivo stimulation in the
74 presence of IL-18 (Fig. 2e-g, Extended Data Fig. 2g). The frequency of $IFN\gamma^{+}$ NK cells was higher
75 in *Il1r8*$^{-/-}$ total NK cells and in all NK cell subsets. Thus, IFNγ production was enhanced
76 independently of the NK cell maturation state. Analysis of competitive bone marrow chimeras
77 revealed that IL-1R8 regulates NK cell differentiation in a cell-autonomous way (Extended Data
78 Fig. 2h-k). Along the same line, co-culture experiments of NK cells with LPS- or CpG-primed
79 dendritic cells (DCs) showed that *Il1r8*$^{-/-}$ NK cells produced higher IFNγ levels irrespectively of the
80 DC genotype (Extended Data Fig. 2l).

81 IL-18 is a member of the IL-1 family, which plays an important role in NK cell

82 differentiation and function[1,14]. Enhanced NK cell maturation and effector function in *Il1r8*$^{-/-}$ mice
83 was abolished by IL-18 blockade or genetic deficiency but unaffected by IL-1R1-deficiency (Fig.
84 2h, 2i, Extended Data Fig. 3a, 3b). Cohousing and antibiotic treatment had no impact, thus
85 excluding a role of microbiota[15] in the phenotype of *Il1r8*$^{-/-}$ mice (Extended Data Fig. 3c, 3d).

86 The results reported above suggested that IL-1R8 regulated the IL-18 signaling pathway in
87 NK cells and indeed, increased phospho-IRAK4/IRAK4 ratio was induced by IL-18 in *Il1r8*$^{-/-}$ NK
88 cells compared to wild type NK cells, indicating unleashed early signaling downstream of MyD88
89 and myddosome formation (Fig. 2j), consistently with the proposed molecular mode of action of IL-
90 1R8[1,9,16]. Indeed, by stimulated emission depletion (STED) microscopy, we observed clustering of
91 IL-1R8 and IL-18Rα (Extended Data Fig. 3e), in line with previous studies[9]. IL-1R8-deficiency
92 also led to enhanced IL-18-dependent phosphorylation of S6 and JNK in NK cells, suggesting that
93 IL-1R8 inhibited IL-18-dependent activation of the mTOR and JNK pathways (Fig. 2j), which
94 control NK cell metabolism, differentiation and activation[17,18].

95 To obtain a deeper insight into the impact of IL-1R8 deficiency on NK cell function and on
96 the response to IL-18, RNA-seq analysis was conducted. IL-1R8 deficiency had a profound impact
97 on the resting transcriptional profile of NK cells and on top on responsiveness to IL-18 (Fig. 2k,
98 Extended Data Fig. 4a and Supplementary Table 1). The profile of IL-1R8 deficient cells includes
99 activation pathways (e.g. MAPK), adhesion molecules involved in cell-to-cell interactions and
100 cytotoxicity (ICAM-1), and increased production of selected chemokines (CCL4). The latter may
101 represent an NK cell based amplification loop of leukocyte recruitment, including NK cells
102 themselves.

103 To investigate the role of IL-1R8 in human NK cells (Fig. 1a, 1b), we first retrospectively
104 analyzed its expression in relation to responsiveness to a combination of IL-18 and IL-12 in normal
105 donors. We observed an inverse correlation between IL-1R8 levels and IFNγ production by
106 peripheral blood NK cells (r^2=0.7969, p=0.0012) (Fig. 2l). In addition, IL-1R8 partial silencing in
107 peripheral blood NK cells with small interfering RNA (siRNA) was associated with a significant

108 increase in IFNγ production (Fig. 2m) and upregulation of CD69 expression (not shown). These
109 results suggest that in human NK cells as in murine counterparts IL-1R8 serves as a negative
110 regulator of activation and that its inactivation unleashes human NK cell effector function.

111 In an effort to assess the actual relevance of IL-1R8-mediated regulation of NK cells,
112 anticancer and antiviral resistance were examined. The liver is characterized by a high frequency of
113 NK cells[19]. Therefore we focused on liver carcinogenesis. In a model of diethylnitrosamine (DEN)-
114 induced hepatocellular carcinoma (HCC), IL-1R8-deficient male and female mice[20] were protected
115 against the development of lesions, in terms of macroscopic number, size (Fig. 3a, Extended Data
116 Fig. 5a, 5b) and histology (not shown). The percentage and absolute number of NK cells, and the
117 percentage of IFNγ^{+} NK cells were higher in *Il1r8*$^{-/-}$ HCC-bearing mice (Fig. 3b, 3c, Extended Data
118 Fig. 5c). Finally, increased levels of cytokines involved in anti-tumor immunity (e.g. IFNγ) and a
119 reduction of pro-inflammatory cytokines associated with tumor promotion (IL-6, TNFα, IL-1β,
120 CCL2, CXCL1) were observed (Extended Data, Table 1). Most importantly, the depletion of NK
121 cells abolished the protection against liver carcinogenesis observed in *Il1r8*$^{-/-}$ mice (Fig. 3d and
122 Extended Data Fig. 5d).

123 Evidence suggests that NK cells can inhibit hematogenous cancer metastasis[5]. In a model of
124 sarcoma (MN/MCA1) spontaneous lung metastasis, *Il1r8*$^{-/-}$ mice showed a reduced number of
125 hematogenous metastasis, whereas primary tumor growth was unaffected (Fig. 3e, Extended Data
126 Fig. 5e, 5f). The frequency of total and mature CD27^{low} NK cells was higher in *Il1r8*$^{-/-}$ lungs (Fig.
127 3f and not shown). Assessment of lung metastasis at sacrifice and *in vivo* imaging analysis (Fig. 3g,
128 Extended Data Fig. 5e) showed that the protection was completely abolished in NK cell-depleted
129 *Il1r8*$^{-/-}$ mice. In addition, IL-18 or IFNγ neutralization abolished or dramatically reduced the
130 protection against metastasis observed in *Il1r8*$^{-/-}$ mice (Extended Data Fig. 5g). In contrast,
131 depletion of CD4^{+}/CD8^{+} cells or IL-17A, or deficiency of IL-1R1 (involved in TH17 development),
132 did not affect the phenotype (Extended Data Fig. 5h, 5i).

133 Liver metastasis is a major problem in the progression of colorectal cancer. We therefore

134 assessed the potential of *Il1r8*$^{-/-}$ NK cells to protect against liver metastasis using the MC38 colon
135 carcinoma line[21]. As shown in Fig. 3h, *Il1r8*$^{-/-}$ mice were protected against MC38 colon carcinoma
136 liver metastasis. In addition, IL-18 genetic deficiency abrogated the protection against liver
137 metastasis observed in *Il1r8*$^{-/-}$ mice (Extended Data Fig. 5j), thus indicating that the IL-1R8-
138 dependent control of MC38-derived liver metastasis occurs through the IL-18/IL-18R axis. To
139 assess the primary role of *Il1r8*$^{-/-}$ NK cells in the cancer protection, adoptive transfer was used
140 (Extended Data Fig. 5k-m). Adoptive transfer of *Il1r8*$^{+/+}$ NK cells had no effect on lung and liver
141 metastasis. In contrast, adoptive transfer of *Il1r8*$^{-/-}$ NK cells significantly and dramatically reduced
142 the number and volume of lung and liver metastasis (Fig. 3i, 3j, Extended Data Fig. 5n). Given the
143 natural history and clinical challenges of colorectal cancer, this observation has potential
144 translational implications. Thus, IL-1R8 genetic inactivation unleashes NK cell mediated resistance
145 to carcinogenesis in the liver and amplifies the anti-metastatic potential of these cells in liver and
146 lung in a NK cell-autonomous manner.

147 Finally we investigated whether IL-1R8 impacts on NK cell antiviral activity, focusing on
148 murine cytomegalovirus (MCMV) infection[22]. As shown in Fig. 4a, liver viral titers were lower in
149 *Il1r8*$^{-/-}$ compared to *Il1r8*$^{+/+}$ mice, indicating that IL-1R8-deficiency was associated with a more
150 efficient control of MCMV infection. The frequency of IFNγ^{+} NK cells and degranulation (i.e.
151 frequency of CD107a^{+} NK cells) were significantly higher in the spleen and liver of *Il1r8*$^{-/-}$ mice on
152 day 1.5 post infection (Fig. 4b). On day 4.5 post infection, IFNγ^{+} and CD107a^{+} NK cells were
153 strongly reduced, in both spleen and liver, as a consequence of better control of viral spread (Fig.
154 4b). Consistently with a more efficient control of the infection, reduced levels of pro-inflammatory
155 cytokines were observed in *Il1r8*$^{-/-}$ mice (Extended Data Fig. 6a). NK cell adoptive transfer
156 experiments were performed in MCMV infected newborn mice that still do not have mature NK
157 cells[12]. As shown in Fig. 4c, the adoptive transfer of *Il1r8*$^{-/-}$ NK cells conferred higher protection
158 compared to *Il1r8*$^{+/+}$ NK cells, with for instance 4 out of 9 mice having no detectable virus titer in
159 the brain.

160 NK cells belong to the complex, diverse realm of innate lymphoid cells[23]. Human and
161 murine non-NK ILCs express IL-1R8 mRNA and protein[24] (and our unpublished data; Camilla
162 Jandus, personal communication). Preliminary experiments were conducted in an effort to assess
163 the role of IL-1R8 in ILC function. In the MCMV infection model, *Il1r8*$^{-/-}$ ILC1 showed increased
164 IFNγ production, but represented a minor population compared to NK cells and 1/30 of *Il1r8*$^{-/-}$ IFNγ
165 producing cells (Fig. 4d) and therefore are unlikely to play a significant role in the phenotype.
166 These results provide initial evidence that IL-1R8 has a regulatory function in ILCs. Further studies
167 are required to assess its actual significance in ILC diverse populations. Collectively, these results
168 indicate that IL-1R8-deficient mice were protected against MCMV infection and that protection
169 was dependent on increased NK cell activation.

170 IL-1R8 deficiency was associated with exacerbated inflammatory and immune reactions
171 under a variety of conditions[1,10]. NK cells engage in bidirectional interactions with macrophages,
172 dendritic cells and other lymphocytes[3,4,25,26]. Therefore the role of NK cells in inflammatory and
173 autoimmune conditions associated with IL-1R8 deficiency[1,10] will need to be examined. IL-1R8
174 deficient mice show increased susceptibility to colitis and colitis-associated azoxymethane (AOM)
175 carcinogenesis[27,28]. The divergent impact on carcinogenesis of IL-1R8 deficiency in the intestine
176 and liver is likely to reflect fundamental, tissue-dictated differences of immune mechanisms
177 involved in carcinogenesis in these different anatomical sites. In particular, high numbers of NK
178 cells are present in the liver[19] and this physiological characteristic of this organ is likely to underlie
179 this apparent divergence.

180 NK cells are generally not credited to play a major role in the control of solid tumors[6].
181 Conversely there is evidence for a role of NK cells in the control of hematogenous lung
182 metastasis[5,29]. The results presented here show that unleashing NK cells by genetic inactivation of
183 IL-1R8 resulted in inhibition of liver carcinogenesis and protection against liver and lung
184 metastasis. IL-1R8-deficient mice show exacerbated TLR and IL-1-driven inflammation[10] and
185 inflammation promotes liver carcinogenesis[30]. Therefore the results presented here are likely an

186 underestimate of the potential against liver primary and metastatic tumors of removal of the NK cell
187 checkpoint IL-1R8. Therefore, NK cells have the potential to restrain solid cancer and metastasis,
188 provided critical, validated checkpoints such as IL-1R8 are removed and the tissue immunological
189 landscape is taken into account.
190
191
192 **References**
193 1 Garlanda, C., Dinarello, C. A. & Mantovani, A. The interleukin-1 family: back to the future.
194 *Immunity* **39**, 1003-1018, (2013).
195 2 Di Santo, J. P. Natural killer cell developmental pathways: a question of balance. *Annu Rev*
196 *Immunol* **24**, 257-286, (2006).
197 3 Vivier, E. *et al.* Innate or adaptive immunity? The example of natural killer cells. *Science*
198 **331**, 44-49, (2011).
199 4 Bellora, F. *et al.* Human NK cells and NK receptors. *Immunol Lett* **161**, 168-173, (2014).
200 5 Guillerey, C., Huntington, N. D. & Smyth, M. J. Targeting natural killer cells in cancer
201 immunotherapy. *Nat Immunol* **17**, 1025-1036, (2016).
202 6 Stojanovic, A. & Cerwenka, A. Natural killer cells and solid tumors. *J Innate Immun* **3**, 355-
203 364, (2011).
204 7 Gismondi, A., Stabile, H., Nisti, P. & Santoni, A. Effector Functions of Natural Killer Cell
205 Subsets in the Control of Hematological Malignancies. *Front Immunol* **6**, 567, (2015).
206 8 Gulen, M. F. *et al.* The receptor SIGIRR suppresses Th17 cell proliferation via inhibition of
207 the interleukin-1 receptor pathway and mTOR kinase activation. *Immunity* **32**, 54-66,
208 (2010).
209 9 Nold-Petry, C. A. *et al.* IL-37 requires the receptors IL-18Ralpha and IL-1R8 (SIGIRR) to
210 carry out its multifaceted anti-inflammatory program upon innate signal transduction. *Nat*
211 *Immunol* **16**, 354-365, (2015).

212 10 Garlanda, C., Riva, F., Bonavita, E. & Mantovani, A. Negative regulatory receptors of the
213 IL-1 family. *Seminars in immunology* **25**, 408-415, (2013).
214 11 Cooper, M. A. *et al.* Human natural killer cells: a unique innate immunoregulatory role for
215 the CD56(bright) subset. *Blood* **97**, 3146-3151, (2001).
216 12 Chiossone, L. *et al.* Maturation of mouse NK cells is a 4-stage developmental program.
217 *Blood* **113**, 5488-5496, (2009).
218 13 Kim, S. *et al.* In vivo developmental stages in murine natural killer cell maturation. *Nat*
219 *Immunol* **3**, 523-528, (2002).
220 14 Takeda, K. *et al.* Defective NK cell activity and Th1 response in IL-18-deficient mice.
221 *Immunity* **8**, 383-390, (1998).
222 15 Ganal, S. C. *et al.* Priming of natural killer cells by nonmucosal mononuclear phagocytes
223 requires instructive signals from commensal microbiota. *Immunity* **37**, 171-186, (2012).
224 16 Gong, J. *et al.* Inhibition of Toll-like receptors TLR4 and 7 signaling pathways by SIGIRR:
225 a computational approach. *J Struct Biol* **169**, 323-330, (2010).
226 17 Marcais, A. *et al.* The metabolic checkpoint kinase mTOR is essential for IL-15 signaling
227 during the development and activation of NK cells. *Nat Immunol* **15**, 749-757, (2014).
228 18 Li, C. *et al.* JNK MAP kinase activation is required for MTOC and granule polarization in
229 NKG2D-mediated NK cell cytotoxicity. *Proc Natl Acad Sci U S A* **105**, 3017-3022, (2008).
230 19 Peng, H. & Tian, Z. Re-examining the origin and function of liver-resident NK cells. *Trends*
231 *Immunol* **36**, 293-299, (2015).
232 20 Naugler, W. E. *et al.* Gender disparity in liver cancer due to sex differences in MyD88-
233 dependent IL-6 production. *Science* **317**, 121-124, (2007).
234 21 Dupaul-Chicoine, J. *et al.* The Nlrp3 Inflammasome Suppresses Colorectal Cancer
235 Metastatic Growth in the Liver by Promoting Natural Killer Cell Tumoricidal Activity.
236 *Immunity* **43**, 751-763, (2015).

237 22 Lisnic, B., Lisnic, V. J. & Jonjic, S. NK cell interplay with cytomegaloviruses. *Curr Opin*
238 *Virol* **15**, 9-18, (2015).
239 23 Eberl, G., Colonna, M., Di Santo, J. P. & McKenzie, A. N. Innate lymphoid cells. Innate
240 lymphoid cells: a new paradigm in immunology. *Science* **348**, aaa6566, (2015).
241 24 Shih, H. Y. *et al.* Developmental Acquisition of Regulomes Underlies Innate Lymphoid Cell
242 Functionality. *Cell* **165**, 1120-1133, (2016).
243 25 Bellora, F. *et al.* M-CSF induces the expression of a membrane-bound form of IL-18 in a
244 subset of human monocytes differentiating in vitro toward macrophages. *Eur J Immunol* **42**,
245 1618-1626, (2012).
246 26 Martin-Fontecha, A. *et al.* Induced recruitment of NK cells to lymph nodes provides IFN-
247 gamma for T(H)1 priming. *Nat Immunol* **5**, 1260-1265, (2004).
248 27 Garlanda, C. *et al.* Increased susceptibility to colitis-associated cancer of mice lacking TIR8,
249 an inhibitory member of the interleukin-1 receptor family. *Cancer Res* **67**, 6017-6021,
250 (2007).
251 28 Xiao, H. *et al.* The Toll-interleukin-1 receptor member SIGIRR regulates colonic epithelial
252 homeostasis, inflammation, and tumorigenesis. *Immunity* **26**, 461-475, (2007).
253 29 Morvan, M. G. & Lanier, L. L. NK cells and cancer: you can teach innate cells new tricks.
254 *Nat Rev Cancer* **16**, 7-19, (2016).
255 30 He, G. & Karin, M. NF-kappaB and STAT3 - key players in liver inflammation and cancer.
256 *Cell Res* **21**, 159-168, (2011).
257

258 **Acknowledgments**

259 We thank N. Polentarutti, G. Benigni, M. Erreni, F. Colombo, V. Juranić Lisnić, D. Kvestak for
260 technical assistance, Prof. M. Nebuloni for HCC histology, Dr. A. Doni for STED images, Dr. F.
261 Ficara, Dr. R. Carriero and Prof. D. Mavilio for discussion.

262 The contribution of the European Commission (ERC project PHII-669415; FP7 project 281608
263 TIMER; ESA/ITN, H2020-MSCA-ITN-2015-676129), Ministero dell'Istruzione, dell'Università e
264 della Ricerca (MIUR) (project FIRB RBAP11H2R9), Associazione Italiana Ricerca sul Cancro
265 (AIRC IG-19014 and AIRC 5x1000 -9962), Fondazione CARIPLO (project 2015-0564), and the
266 Italian Ministry of Health is gratefully acknowledged. MM received an EFIS short-term fellowship
267 to perform viral infection experiments in SJo's laboratory. The authors declare no competing
268 financial interests.

269 **Author contributions**

270 E.B. and M.M. played a key role in designing and conducting most experiments and drafted the
271 manuscript. F.R., M.B., F.G., E.M. provided technological support in *in vivo* experiments. A.P.,
272 S.Ja., B.P. and G.B. contributed to the experimental design and in *in vivo* experiments. S.Z.
273 contributed to RNA-seq analysis. S.Jo. and A.S. contributed to the experimental design and
274 supervision of the study. C.G. and A.M. contributed to the experimental design and supervision of
275 the study, and suggested the role of IL-1R8 as a novel checkpoint inhibitor of NK cells.

276 **Author Information**

277 Reprints and permissions information is available at www.nature.com/reprints.
278 Authors declare no Competing financial interests.
279 Correspondence and requests for materials should be addressed to
280 cecilia.garlanda@humanitasresearch.it or alberto.mantovani@humanitasresearch.it

281

282

283 **Figures**

284 **Figure 1. Expression of IL-1R8 in human and murine NK cells**

285 (a, b) IL-1R8 protein expression in human primary NK cells and other leukocytes (a) and NK cell

286 maturation stages (b).

287 (c, d) Il-1r8 mRNA expression in murine primary NK cells and other leukocytes (c) and in sorted

288 splenic NK cell subsets (c).

289 *p < 0.05, **p < 0.01, ***p < 0.001 One-way ANOVA. Mean ± SEM.

290

291 **Figure 2. NK cell differentiation and function in IL-1R8-deficient mice**

292 (a, b) NK cell frequency and absolute number among leukocytes in $\mathit{Il1r8}^{+/+}$ and $\mathit{Il1r8}^{-/-}$ mice.

293 (c, d) NK cell subsets (c) and $KLRG1^{+}$ NK cells (d).

294 (e-g) IFNγ (e), Granzyme B (f) and FasL (g) expression in stimulated NK cells.

295 (h) Splenic $CD27^{low}$ NK cell frequency upon IL-18 *in vivo* depletion.

296 (i) IFNγ production by $\mathit{Il1r8}^{+/+}$ and $\mathit{Il1r8}^{-/-}$ NK cells upon co-culture with CpG-primed $\mathit{Il1r8}^{+/+}$ DCs

297 and IL-18 blockade.

298 (j) IRAK4, S6 and JNK phosphorylation in NK cells upon stimulation with IL-18.

299 (k) RNA-seq analysis of resting and IL-18-activated NK cells. Differentially expressed (p<0.05)

300 genes are shown. FC: fold change.

301 (l) Correlation between IL-1R8 expression and IFNγ production in human peripheral blood NK

302 cells.

303 (m) IL-1R8 expression and IFNγ production in human NK cells 7 days after transfection with

304 control siRNA or IL-1R8-specific siRNA in duplicate.

305 (a-l) *p < 0.05, **p < 0.01, ***p < 0.001 between selected relevant comparisons, two-tailed

306 unpaired Student's t test or Mann-Whitney test; (k) r: Pearson correlation coefficient; Mean ± SEM.

307

308 **Figure 3. NK cell-mediated protection against liver carcinogenesis and metastasis in IL-1R8-**
309 **deficient mice**
310 (a) Macroscopic score of liver lesions in male *Il1r8*$^{+/+}$ and *Il1r8*$^{-/-}$ mice 6, 8, 10 and 12 months after
311 DEN injection.
312 (b) Frequency and representative histological quantification of NK cell infiltrate in liver of tumor
313 bearing mice. (20X, bar = 100μm).
314 (c) Frequency of IFNγ^{+} NK cells in liver of tumor bearing mice.
315 (d) Macroscopic score of liver lesions in male mice upon NK cell depletion.
316 (e) Number of spontaneous lung metastasis.
317 (f) NK cell frequency in the lungs of MN/MCA1 tumor bearing mice.
318 (g) Number of lung metastasis in MN/MCA1 tumor bearing mice upon NK cell depletion.
319 (h) Number of liver metastasis in MC38 colon carcinoma bearing mice.
320 (i,j) Number of lung (i) and liver (j) metastasis of *Il1r8*$^{+/+}$ mice after adoptive transfer of *Il1r8*$^{+/+}$
321 and *Il1r8*$^{-/-}$ NK cells.
322 (a, d) Representative images of female livers are shown.
323 (a-j) *p < 0.05, **p < 0.01, ***p < 0.001 between selected relevant comparisons, two-tailed
324 unpaired Student's t test. Mean ± SEM.
325
326 **Figure 4. NK cell-mediated antiviral resistance in IL-1R8-deficient mice**
327 (a) Viral titer in livers of *Il1r8*$^{+/+}$ and *Il1r8*$^{-/-}$ infected mice.
328 (b) Frequency of IFNγ^{+} and CD107a^{+} NK cells of infected mice.
329 (c) Viral titers in newborn wild type mice upon adoptive transfer of *Il1r8*$^{+/+}$ and *Il1r8*$^{-/-}$ NK cells (7
330 days post infection).
331 (d) Frequency of IFNγ^{+} cells in the liver of MCMV infected mice.

332 (a-d) $*p < 0.05$, $**p < 0.01$, $***p < 0.001$, two-tailed Mann-Whitney test (a, c) or unpaired

333 Student's t test (b, d). Median (a, c). Mean ± SEM (b, d). DL: detection limit. Day p.i.: day post

334 infection.

335

336 **Methods**

337 **Animals.** All female and male mice used were on a C57BL/6J genetic background and 8-12 weeks-
338 old, unless specified. Wild-type mice were obtained from Charles River Laboratories, Calco, Italy
339 or were littermates of *Il1r8*$^{-/-}$ mice. IL-1R8-deficient mice were generated as described[31]. *Il1r1*$^{-/-}$
340 mice were purchased from The Jackson Labs, Bar Harbor ME, USA. All colonies were housed and
341 bred in the SPF animal facility of Humanitas Clinical and Research Center in individually
342 ventilated cages. *Il1r1*$^{-/-}$/*Il1r8*$^{-/-}$ mice were generated by crossing *Il1r1*$^{-/-}$ and *Il1r8*$^{-/-}$ mice. *Il18*$^{-/-}$
343 /*Il1r8*$^{-/-}$ were generated by crossing *Il18*$^{-/-}$ and *Il1r8*$^{-/-}$ mice. Mice were randomized based on sex,
344 age and weight.

345 Procedures involving animals handling and care were conformed to protocols approved by the
346 Humanitas Clinical and Research Center (Rozzano, Milan, Italy) in compliance with national (D.L.
347 N.116, G.U., suppl. 40, 18-2-1992 and N. 26, G.U. March 4, 2014) and international law and
348 policies (EEC Council Directive 2010/63/EU, OJ L 276/33, 22-09-2010; National Institutes of
349 Health Guide for the Care and Use of Laboratory Animals, US National Research Council, 2011).
350 The study was approved by the Italian Ministry of Health (approvals n. 43/2012-B, issued on the
351 08/02/2012 and n. 828/2015-PR, issued on the 07/08/2015). All efforts were made to minimize the
352 number of animals used and their suffering. In most *in vivo* experiments, the investigators were
353 unaware of the genotype of the experimental groups. Sample size was defined in order to detect
354 differences of 20% or grater between the groups (10% significance level and 80% power).

355

356 **Human primary cells.** Human peripheral mononuclear cells (PBMCs) were isolated from
357 peripheral blood of healthy donors, upon approval by Humanitas Research Hospital Ethical
358 Committee. PBMCs were obtained through a Ficoll density gradient centrifugation (GE Healthcare
359 Biosciences). NK cells were then purified by a negative selection, using a magnetic cell-sorting
360 technique according to the protocols given by the manufacturer (EasySep™ Human NK Cell
361 Enrichment Kit, Stem Cell Technology). Human monocytes were obtained from peripheral blood of

362 healthy donors by two-step gradient centrifugation, first by Ficoll and then by Percoll (65% iso-
363 osmotic; Pharmacia, Uppsala, Sweden). Residual T and B cells were removed from monocyte
364 fraction by plastic adherence. Monocytes were cultured in RPMI-1640 medium supplemented with
365 10% Fetal Bovine Serum (FBS), 1% L-Glutamine, 1% Pen/Strept and 100 ng/ml M-CSF
366 (Peprotech) for 7 days in order to generate resting macrophages. T and B cells were obtained from
367 peripheral blood of healthy donors using RosetteSep™ Human T Cell Enrichment Cocktail and
368 RosetteSep™ Human B Cell Enrichment Cocktail (Stem Cell Technology), following the
369 manufacturer's instructions. Neutrophils were enriched from Ficoll–isolated granulocytes, using
370 EasySep™ Human Neutrophil Enrichment Kit (StemCell Technologies), according to the
371 manufacturer's instructions.
372 To analyse pluripotent haematopoietic stem cells (HSC) and NK cell precursors (NKP), human
373 Bone Marrow mononuclear cells were collected from Humanitas Biobank, upon approval by
374 Humanitas Research Hospital Ethical Committee (Authorization 1516, issued on February 26,
375 2016). Frozen samples were thawed and vitality was assessed by trypan blue and Aqua LIVE/Dead-
376 405 nm staining (Invitrogen), before flow cytometry analysis.
377 Informed consent was obtained from all subjects.
378

379 **FACS analysis.** Single-cell suspensions of BM, blood, spleen, lung and liver were obtained and
380 stained. Representative NK cell gating strategy is reported in Supplementary Fig. 1.
381 Foxp3/Transcription Factor Staining Buffer Set (eBioscience) was used for intracellular staining of
382 Granzyme B and Perforin. Cytofix/Cytoperm (BD Biosciences) was used for intracellular staining
383 of IFNγ. Liver ILC1 were identified as NK1.1^{+}CD3^{-}CD49a^{+}CD49b^{-} cells. Formalin 4% and
384 Methanol 100% were used for intracellular staining of IRAK4, pIRAK4, pS6 and JNK. The
385 following murine antibodies were used: CD45-BV605, -BV650 or -PerCp-Cy5.5 (Clone 30-F11);
386 CD45.1-BV650 (Clone A20); CD45.2-APC, -BV421 (Clone 104); CD3e-PerCP-Cy5.5 or -APC
387 (Clone 145-2C11); CD19-PerCP-Cy5.5, -eFluor450 (Clone 1D3); NK1.1-PE, -APC, -eFluor450 or

388 –Biotin (Clone PK136); CD11b-BV421, -BV450, -BV785 (Clone M1/70); CD27-FITC or –APC-
389 eFluor780 (Clone LG.7F9); CD4-FITC (Clone RM 4-5); CD8-PE (Clone 53-6.7); KLRG-1-BV421
390 (Clone 2F1); NKG2D-APC (Clone CX5); DNAM-1-APC (Clone 10E5); Ly49H-PECF594 (Clone
391 3D10); Granzyme B-PE (Clone NGZB); Perforin-PE (Clone eBioOMAK-D); IFNγ-Alexa700 or -
392 APC (Clone XMG1.2); CD107a-Alexa647 (Clone 1D4B); FasL-APC (Clone MFL3); Lineage Cell
393 Detection Cocktail-Biotin; Sca-1-FITC (Clone D7); CD117-PE or -Biotin (Clone 3C11); CD127-
394 eFluor450 (Clone A7R34); CD135-APC or –Biotin (Clone A2F10.1); CD244-PE (Clone 2B4);
395 CD122-PE-CF594 (Clone TM-Beta1); CD49b-PE-Cy7 or Biotin (Clone DX5), CD49a-APC (Clone
396 Ha31/8), from BD Bioscience, eBioscience, BioLegend or Miltenyi Biotec. The following human
397 antibodies were used: CD56-PE (Clone CMSSB); CD3-FITC (Clone UCHT1); CD16-Pacific Blue
398 (Clone 3G8); CD34-PE-Vio770 (Clone AC136); CD117-BV605 (Clone 104D2); NKp46-BV786
399 (Clone 9E2/NKp46); CD45-PerCP (Clone 2D1); CD19-APC-H7 (Clone SJ25C1); CD14-APC-H7
400 (Clone M5E2); CD66b-APC-Vio770 (Clone REA306), from BD Bioscience, eBioscience or
401 Miltenyi Biotec. Biotinylated anti-hSIGIRR (R&D Systems) and Streptavidin-Alexa647
402 (Invitrogen™) were used to stain IL-1R8 in human cells. Human NKT cells were detected using
403 PE-CD1d tetramers loaded with αGalCer (ProImmune, Oxford, UK). Antibodies to detect protein
404 phosphorylation were as follows: p-IRAK4 Thr345/Ser346 (Clone D6D7), IRAK4, p-S6-Alexa647
405 Ser235/236 (Clone D57.2.2E); p-SAPK/JNK Thr183/Tyr185 (Clone 81E11), from Cell Signaling
406 Technology. A Goat anti-Rabbit-Alexa647 secondary antibody (Invitrogen™) was used to stain p-
407 IRAK4, IRAK4 and p-SAPK/JNK. Results are reported as mean fluorescence intensity (MFI)
408 normalized on isotype control or fluorescence minus one (FMO). Cell viability was determined by
409 Aqua LIVE/Dead-405 nm staining (Invitrogen) or Fixable Viability Dye (FVD) eFluor® 780
410 (eBioscience), negative cells were considered viable. Cells were analyzed on LSR Fortessa or
411 FACSVerse (BD Bioscience). Data were analyzed with FlowJo software (Treestar).
412
413 **Quantitative PCR.** Total RNA was extracted using Trizol reagent (Invitrogen) following the

414 manufacturer's recommendations. RNA was further purified using miRNeasy RNA isolation kit
415 (QIAGEN) or Direct-zol™ RNA MiniPrep Plus (Zymo Research). cDNA was synthesized by
416 reverse transcription using High Capacity cDNA archive kit (Applied Biosystems) and quantitative
417 real-time PCR was performed using the SybrGreen PCR Master Mix (Applied Biosystems) in a
418 CFX96 Touch™ Real-Time PCR Detection System (Bio-Rad). PCR reactions were carried out with
419 10 ng of DNA. Data were analyzed with the Δ^2CT method. Data were normalized based on
420 GAPDH, βactin or 18S expression, as indicated, determined in the same sample. Analysis of all
421 samples was performed in duplicate. Primers were designed according to the published sequences
422 and listed as follows: *s18/S18*: forward 5'-ACT TTC GAT GGT AGT CGC CGT-3', reverse 5'-
423 CCT TGG ATG TGG TAG CCG TTT-3'; *Gapdh/GAPDH*: forward 5'-GCA AAG TGG AGA TTG
424 TTG CCA T-3', reverse 5'-CCT TGA CTG TGC CGT TGA ATT T-3'; *βactin/βACTIN*: forward 5'-
425 CCC AAG GCC AAC CGC GAG AAG AT-3', reverse 5'- GTC CCG GCC AGC CAG GTC CAG
426 -3'; *il1r8*: forward 5'- AGA GGT CCC AGA AGA GCC AT-3', reverse 5'- AAG CAA CTT CTC
427 TGC CAA GG-3'; *IL1R8*: forward 5'- ATG TCA AGT GCC GTC TCA ACG -3', reverse 5'- GCT
428 GCG GCT TTA GGA TGA AGT-3'; *il1r1*: forward 5'- TGC TGT CGC TGG AGA TTG AC -3',
429 reverse 5'- TGG AGT AAG AGG ACA CTT GCG AA -3'; *il1r2*: forward 5'- AGT GTG CCC
430 TGA CCT GAA AGA -3', reverse 5'- TCC AAG AGT ATG GCG CCC T -3'; *il1r3*: forward 5'-
431 GGC TGG CCC GAT AAG GAT -3', reverse 5'- GTC CCC AGT CAT CAC AGC G -3'; *il1r4*:
432 forward 5'- GAA TGG GAC TTT GGG CTT TG -3', reverse 5'- GAC CCC AGG ACG ATT TAC
433 TGC -3'; *il1r5*: forward 5'- GCT CGC CCA GAG TCA CTT TT -3', reverse 5'- GCG ACG ATC
434 ATT TCC GAC TT -3'; il1r6: forward 5'- GCT TTT CGT GGC AGC AGA TAC -3', reverse 5'-
435 CAG ATT TAC TGC CCC GTT TGT T -3'; 16S: forward 5'- AGA GTT TGA TCC TGG CTC
436 AG -3', reverse 5'- GGC TGC TGG CAC GTA GTT AG -3'.
437

438 **Purification of murine leukocytes.** Splenic NK cells and bone marrow neutrophils were MACS
439 enriched according to manufacturer's instructions (Miltenyi Biotec). Purity of NK cells was about

440 90% as determined by FACS. Purity of neutrophils was ≥ 97.5%. NK cells were stained (CD45-
441 BV650, NK1.1-PE, CD3e-APC, CD11b-BV421, CD27-FITC) and sorted on a FACSAria cell sorter
442 (BD Bioscience) to obtain high purity NK cells and NK cell populations ($CD11b^{low}CD27^{low}$,
443 $CD11b^{low}CD27^{high}$, $CD11b^{high}CD27^{high}$ and $CD11b^{high}CD27^{low}$). Splenic B and T lymphocytes were
444 stained (CD45-PerCP, CD3e-APC, CD4-FITC, CD8-PE, CD19-eFluor450) and sorted. Purity of
445 each population was ≥ 98%. Resulting cells were processed for mRNA extraction or used for
446 adoptive transfer or co-culture experiments. *In vitro*-derived macrophages were obtained from bone
447 marrow total cells. Bone marrow cells were cultured in RPMI-1640 medium supplemented with
448 10% Fetal Bovine Serum (FBS), 1% L-Glutamine, 1% Pen/Strept and 100 ng/ml M-CSF
449 (Peprotech) for 7 days in order to generate resting macrophages. Bone marrow cells were cultured
450 in RPMI-1640 medium supplemented with 10% Fetal Bovine Serum (FBS), 1% L-Glutamine, 1%
451 Pen/Strept and 20 ng/ml GM-CSF (Peprotech) for 7 days in order to generate DCs.
452
453 **Confocal microscopy:** Murine splenic NK cells were MACS enriched, let adhere on poly-D-Lysine
454 (Sigma-Aldrich) coated coverslips, fixed with 4% PFA, permeabilized with 0.1% Triton X-100,
455 incubated with blocking buffer (5% normal donkey serum (Sigma-Aldrich), 2% BSA, 0.05%
456 Tween). Cells were then stained with biotin-conjugated goat polyclonal anti-SIGIRR antibody or
457 biotin-conjugated normal goat IgG as control (both R&D Systems) (10µg/ml) followed by Alexa
458 Fluor 488–conjugated donkey anti-goat IgG antibody (Molecular Probes) and DAPI (Invitrogen).
459 Coverslips were mounted with the antifade medium FluorPreserve Reagent (EMD Millipore) and
460 analyzed with an Olympus Fluoview FV1000 laser scanning confocal microscope with oil
461 immersion lens 40× (N.A.1.3).
462
463 **Stimulated emission depletion (STED) microscopy**
464 Human NK cells were enriched and let adhere on poly-D-Lysine (Sigma-Aldrich) coated coverslips,
465 stimulated with IL-18 (50 ng/ml; 1 min, 5 min, 10 min), fixed with 4% PFA, incubated with 5%

466 normal donkey serum (Sigma-Aldrich), 2% BSA, 0.05% Tween in PBS2+ (pH 7.4) (blocking
467 buffer), and then with biotin-conjugated goat polyclonal anti-human IL-1R8 antibody or biotin-
468 conjugated normal goat IgG (all from R&D Systems) and mouse monoclonal anti-IL-18Rα (Clone
469 70625; R&D System) or mouse IgG1 (Invitrogen), all diluted at 5μg/ml in blocking buffer,
470 followed by Alexa Fluor 488– conjugated donkey anti-goat IgG antibody and Alexa Fluor 555
471 donkey anti-mouse IgG antibody (both from Molecular Probes). Mowiol was used as mounting
472 medium. STED xyz images were acquired in a unidirectional mode with a Leica SP8 STED3X
473 confocal microscope system. Alexa Fluor 488 was excited with a 488nm Argon Laser and emission
474 collected from 505 to 550 nm applying a gating between 0.4 to 7ns to avoid collection of reflection
475 and autofluorescence. Alexa Fluor 555 was excited with a 555/547nm-tuned white light laser
476 (WLL) and emission collected from 580 to 620 nm. Line sequential acquisition was applied to
477 avoid fluorescence overlap. The 660nm CW-depletion laser (80% of power) was used for both
478 excitations. Images were acquired with Leica HC PL APO 100x/1.40 oil STED White objective at
479 572.3mAU. CW-STED and gated CW-STED were applied to Alexa-488nm and Alexa Fluor 555,
480 respectively. Collected images were de-convolved with Huygens Professional software.
481

482 **3′-mRNA Sequencing and Analysis**

483 Splenic NK cells (from 6 mice per genotype and pooled in pairs) were purified as described above
484 and stimulated with IL-18 (MBL) (20 ng/ml for 4 h). RNA was prepared as described above. The
485 QuantSeq 3′mRNA-seq Library Prep Kit for Illumina (Lexogen) was used to generate libraries,
486 which were sequenced on the NextSeq (Illumina; 75 bp PE). The fastq sequence files were
487 assessed using the fastqc program. The reads were first trimmed using bbduk in the bbmap suite of
488 software[32] to remove the first 12 bases and a contaminant kmer discovery length of 13 was used for
489 contaminant removal. Regions of length 20 or above with average quality of less than 10 were
490 trimmed from the end of the read. The reads were then trimmed to remove trailing polyG and polyA
491 runs using cutadapt[33] and the quality of the remaining reads reassessed with fastqc. The trimmed

492 reads were aligned to the mm10 genomic reference and reads assigned to features in the mm10
493 annotation using the STAR program[34]. Differential expression analysis was performed using the
494 generalized linear model (GLM) functions in the R/bioconductor[35] edgeR package[36] with TMM
495 normalization. Gene set analysis was performed using the romer[37] function in the R/bioconductor
496 package limma[38]. Metascape (http://metascape.org) was used to enrich genes for GO biological
497 processes, KEGG Pathway and Reactome Gene Sets.
498
499 **Measurement of cytokines:** BD Cytometric Bead Array (CBA) mouse inflammation kit (BD) or
500 Duoset ELISA kits (R&D System) were used to measure cytokines.
501
502 ***In vitro* functional assays.** Total murine splenocytes or enriched murine or human NK cells were
503 cultured in RPMI-1640 medium supplemented with 10% Fetal Bovine Serum (FBS) 1% L-
504 Glutamine, 1% Pen/Strept and treated with IL-2, IL-12, IL-15 (Peprotech), IL-18 (MBL), IL-1β
505 (Peprotech) and PMA-Ionomycin (Sigma-Aldrich), as specified. FasL expression was evaluated
506 upon treatment for 45 minutes with IL-18 (50 ng/ml), IL-15 (50 ng/ml), IL-2 (20 ng/ml) and IL-12
507 (10 ng/ml). IFNγ production was analysed upon 16 hours of treatment with IL-12 (20 ng/ml) and
508 IL-18 (20 ng/ml) or IL-1β (20 ng/ml), by intracellular staining using BD Cytofix/Cytoperm™
509 Fixation/Permeabilization Kit, following the manufacturer's instructions, or by ELISA. Granzyme B
510 and Perforin intracellular staining was performed upon 18 hours of stimulation with IL-12 (10
511 ng/ml), IL-15 (10 ng/ml) and IL-18 (50 ng/ml), using Foxp3/Transcription Factor Staining Buffer
512 Set (eBioscience). CD107a-Alexa647 antibody was added during the 4-hour culture and analysed
513 by flow cytometry. BD GolgiPlug™ (containing Brefeldin) and BD GolgiStop™ (containing
514 Monensin) were added 4 hours prior to intracellular staining. PMA (50 ng/ml)- Ionomycin (1
515 μg/ml) were added 4 hours prior to intracellular staining, when specified.
516 NK-DC co-culture experiments were performed as previously described[39]. DCs were treated with
517 LPS from Escherichia coli O55:B5 (Sigma-Aldrich; 1μg/ml) or CpG ODN 1826 (Invivogen;

518 3μg/ml) and with anti-mIL-18 neutralizing antibody (BioXCell, Clone YIGIF74-1G7; 5μg/ml) or
519 Rat Isotype Control (BioXCell, Clone 2A3).
520 IFNγ and CD107a expression upon viral infection was analyzed by flow cytometry upon 4-hour
521 treatment with BD GolgiPlug™, BD GolgiStop™ and IL-2 (500U/ml).
522 Phosphorylation of IRAK4, S6 and JNK was analyzed upon 15-30 minutes of stimulation with IL-
523 18 (10 ng/ml).
524
525 **Human primary NK cell transfection**: Human NK cells were enriched from peripheral blood of
526 healthy donors and transfected with Dharmacon™ Acell™ siRNA (GE Healthcare) using Accell™
527 delivery medium (GE Healthcare), following the manufacturer's instructions. 1 μM SIGIRR-
528 specific siRNA (On-Target Plus; Dharmacon, GE Healthcare) comprised 250 nM of the four
529 following antisense sequences: I, AGU UUC GCG AGC CGA GAU CUU; II, UAC CAG AGC
530 AGC ACG UUG AUU; III, UGA CCC AGG AGU ACU CGU GUU; IV, CUU CCC GUC GUU
531 UAU CUC CUU (all 5' to 3').
532
533 **Generation of bone marrow chimeras.** *Il1r8*$^{-/-}$ and *Il1r8*$^{+/+}$ mice were lethally irradiated with a
534 total dose of 900 cGy. 2 h later, mice were injected in the retro-orbital plexus with $4x10^6$ nucleated
535 bone marrow cells obtained by flushing of the cavity of freshly dissected femurs from wild type or
536 *Il1r8*$^{-/-}$ donors. Competitive bone marrow chimeric mice were generated by reconstituting recipient
537 mice with 50% CD45.1 *Il1r8*$^{+/+}$ and 50% CD45.2 *Il1r8*$^{-/-}$ bone marrow cells. Recipient mice
538 received gentamycin (0.8 mg/ml in drinking water) starting 10 days before irradiation and for 2
539 weeks after irradiation. NK cells of chimeric mice were analyzed 8 weeks after bone marrow
540 transplantation.
541
542 **Depletion and blocking experiments.** Mice were treated intraperitoneally with 200 μg of specific
543 mAbs (Mouse anti-NK1.1, Clone PK136; Mouse Isotype Control, Clone C1.18.4; Rat anti-mIL-18,

544 Clone YIGIF74-1G7; Rat Isotype Control, Clone 2A3; Rat anti-IFNγ, Clone XMG1.2; Rat IgG1
545 HRPN; Mouse anti-IL-17A, Clone 17F3; Mouse Isotype Control, Clone MOPC-21; Rat anti-
546 CD4/CD8, Clone GK1.5/YTS; Rat Isotype Control, Clone LTF-2 (all from BioXCell)) and then
547 with 100 μg once (anti-NK1.1) or three times (anti-IL-18, anti-IFNγ, anti-IL-17A, anti-CD4/CD8) a
548 week for the entire duration of the experiment.

549

550 **Microflora depletion.** 6-week-old mice were treated every day for 5 weeks by oral gavage with a
551 cocktail of antibiotics [ampicillin (Pfizer) 10 mg/ml, vancomycin (PharmaTech Italia) 10 mg/ml,
552 metronidazol (Società Prodotti Antibiotici) 5 mg/ml and neomycin (Sigma-Aldrich) 10 mg/ml].
553 Control mice were treated with drinking water. A gavage volume of 10 ml/kg body weight was
554 delivered with a stainless steel tube without prior sedation of mice. DNA was isolated from
555 bacterial fecal pellets with PowerSoil® DNA Isolation Kit (MO BIO Laboratories, Inc.) and
556 quantified by spectrophotometry at 260 nm. PCR was performed with 10 ng of DNA using the
557 SybrGreen PCR Master Mix (Applied Biosystems) in a CFX96 Touch™ Real-Time PCR Detection
558 System (Bio-Rad). Data were analyzed with the Δ^2CT method (Applied Biosystems, Real-Time
559 PCR Applications Guide).

560

561 **Cancer models.** Mice were injected intraperitoneally (i.p.) with 25 mg/kg of diethylnitrosamine
562 (DEN, Sigma) at 15 days of age. Mice were sacrificed 6-8-10-12 months later, to analyze liver
563 cancer. Liver cancer score was based on number and volume of lesions (0: no lesions; 1: lesion
564 number<3, or lesion dimension <3mm; 2: lesion number<5, or lesion dimension <5mm; 3: lesion
565 number<10, or lesion dimension <10mm; 4: lesion number<15, or lesion dimension <10mm; 5:
566 lesion number>15, or lesion dimension >10mm). Lung metastasis experiments were performed
567 injecting i.m. the 3-MCA derived mycoplasma-free sarcoma cell line MN/MCA1 (10^5 cells/mouse
568 in 100 μl PBS)[40]. Primary tumor growth was monitored twice weekly, and lung metastases were
569 assessed by *in vivo* imaging and by macroscopic counting at sacrifice 25 days after injection. Liver

570 metastases were generated by injecting intrasplenically $1.5x10^5$ mycoplasma-free colon carcinoma
571 cells (MC38) [21]. Mice were sacrificed 12 days after injection and liver metastasis were counted
572 macroscopically. MC38 cells were received from ATCC just before use. MN/MCA1 cells were
573 authenticated morphologically by microscopy *in vitro* and by histology *ex vivo*. Tumor size limit at
574 which mice were sacrificed was based on major diameter (≤ 2cm).
575
576 **Viral infections**
577 Mice were injected intravenously (i.v.) with 5×10^5 PFU of the tissue culture (TC)-grown virus in
578 PBS. Bacterial artificial chromosome (BAC)-derived MCMV strain MW97.01 has been previously
579 shown to be biologically equivalent to MCMV strain Smith (VR-1399) and is hereafter referred to
580 as wild-type (WT) MCMV[41]. Mice were sacrificed 1.5 and 4.5 days post infection and viral titer
581 was assessed by plaque assay, as previously described[42,43]. Newborn mice were infected i.p. with
582 2000 PFU of the MCMV strain MW97.01 and sacrificed at day 7 post infection. Viral titer was
583 assessed by plaque assay, as previously described[42,43].
584
585 **Adoptive transfer.** 10^6 *Il1r8*$^{+/+}$ or *Il1r8*$^{-/-}$ sorted NK cells were injected i.v. in wild type adult mice
586 5 hours before MN/MCA or MC38 injection, or i.p. in newborn mice 48 hours after MCMV
587 injection. Adoptively transferred NK cell engraftment, proliferative capacity and functionality
588 (IFNγ production and degranulation after *ex vivo* stimulation) were assessed 3 and 7 days after
589 injection.
590
591 ***In vivo* proliferation** was measured using Click-iT® Edu Flow Cytometry Assay Kit (Invitrogen).
592 Edu was injected i.p. (0.5 mg/mouse), mice were sacrificed 24 hours later and cells were stained
593 following the manufacturer's instructions and analyzed by flow cytometry.
594
595 **Immunohistochemistry.** Liver frozen tissues were cut at 8 mm and then fixed with 4% PFA.

596 Endogenous peroxidases were blocked with 0.03% of H_2O_2 for 5 min and unspecific binding sites
597 were blocked with PBS + 1% FBS for 1h. Tissues were stained with polyclonal goat anti mouse
598 NKp46/NCR1 (R&D System) and goat on mouse HRP polymer kit (GHP516, Biocare Medical)
599 was used as secondary antibody. Reactions were developed with 3,3'-Diaminobenzidine (DAB)
600 (Biocare Medical) and then slides were counterstained with hematoxylin. Slides were mounted with
601 eukitt (Sigma-Aldrich). 20X images were analyzed with cell^F software (Olympus).

602

603 ***In vivo* Imaging.** After feeding with AIN-76A alfalfa-free diet (Mucedola srl, Italy) for two weeks,
604 to reduce fluorescence background, mice were intravenously (i.v.) injected with XenoLight
605 RediJect 2-DeoxyGlucosone (DG) (PerkinElmer) and 24 hours later 2-DG fluorescence was
606 measured using Fluorescence Molecular Tomography system (FMT 2000, Perkin Elmer). Acquired
607 images were subsequently analyzed with TrueQuant 3.1 analysis software (Perkin Elmer).

608

609 **Data availability:** The data discussed in this publication have been deposited in NCBI Gene
610 Expression Omnibus and are accessible through GEO Series accession number GSEXXXXX, or
611 from the corresponding author. Figure source data are provided.

612

613 **Statistical analysis.** For animal studies, sample size was defined on the basis of past experience on
614 cancer and infection models, in order to detect differences of 20% or grater between the groups
615 (10% significance level and 80% power). Values were expressed as mean ± SEM or median of
616 biological replicates, as specified. One-way ANOVA or Kruskal-Wallis test were used to compare
617 multiple groups. Two-sided unpaired Student's t test was used to compare unmatched groups with
618 Gaussian distribution and Welch's correction was applied in case of significantly different variance.
619 Mann-Whitney test was used in case of non-Gaussian distribution. ROUT test was applied to
620 exclude outliers. $p \leq 0.05$ was considered significant. Statistics were calculated with GraphPad Prism
621 version 6, GraphPad Software.

622

623 **Statistics and reproducibility**

624 **Figure 1:** a, n=4 (B cells), n=5 (NKT cells), n=9 (T cells) , n=10 (NK cells) donors; b, n=5 donors;
625 c, n=8 (NK cells) or n=4 (T cells) or n=3 (other leukocytes) mice; d, n=5 mice. b, representative
626 experiment out of 6 performed. a, c, d, one experiment performed.

627 **Figure 2:** a, b, n=8 or n=7 (spleen, *Il1r8*$^{+/+}$ liver) or n=6 (*Il1r8*$^{-/-}$ liver) mice; c, n= 6 mice; d, n=9
628 (*Il1r8*$^{+/+}$) or n=6 (*Il1r8*$^{-/-}$) mice; e, n=5 mice; f, n=6 mice; g, n=4 mice; h, n=5 mice; i, n=10 wells; j,
629 n=4 (IRAK4), n=6 or n=5 (S6 *Il1r8*$^{-/-}$) or n=7 (JNK *Il1r8*$^{-/-}$) mice; k, n=3 mice; l, n=9 healthy
630 donors; m, n=4 healthy donors. Representative experiments out of 3 (a, b), 5 (c), 2 (d, j), 4 (e)
631 performed. f-m one experiment performed.

632 **Figure 3:** a, n= 8, 10, 11, 13, 14 mice; b, c, n=6 mice; d, n=10, 12, 13 mice; e, n=10, 11 mice; f,
633 n=5, 6, 7 mice; g, n=9, 10 mice; h, n=5, 6 mice; i, n= 9, 10 or 12 mice; j, n=6 mice. Representative
634 experiments out of 6 (e), 3 (a), 2 (d, f, g, h, i). b, c, j, one experiment performed.

635 **Figure 4:** a,b, n=5 mice; c, n=6, n=9 mice; d, n=4 mice. a, two experiments were performed; b-d,
636 one experiment was performed.

637

638 31 Garlanda, C. *et al.* Intestinal inflammation in mice deficient in Tir8, an inhibitory member
639 of the IL-1 receptor family. *Proc Natl Acad Sci U S A* **101**, 3522-3526, (2004).

640 32 Bushnell, B. Bbmap: A Fast, Accurate, Splice-Aware Aligner (Ernest Orlando Lawrence
641 Berkeley National Laboratory, Berkeley, CA (US), 2014).

642 33 Martin, M. Cutadapt removes adapter sequences from high-throughput sequencing reads.
643 *EMBnet.journal* **17**, (2011).

644 34 Dobin, A. *et al.* STAR: ultrafast universal RNA-seq aligner. *Bioinformatics* **29**, 15-21,
645 (2013).

646 35 Gentleman, R. C. *et al.* Bioconductor: open software development for computational
647 biology and bioinformatics. *Genome Biol* **5**, R80, (2004).

648 36 Robinson, M. D., McCarthy, D. J. & Smyth, G. K. edgeR: a Bioconductor package for
649 differential expression analysis of digital gene expression data. *Bioinformatics* **26**, 139-140,
650 (2010).
651 37 Majewski, I. J. *et al.* Opposing roles of polycomb repressive complexes in hematopoietic
652 stem and progenitor cells. *Blood* **116**, 731-739, (2010).
653 38 Ritchie, M. E. *et al.* limma powers differential expression analyses for RNA-sequencing and
654 microarray studies. *Nucleic Acids Res* **43**, e47, (2015).
655 39 Mingozzi, F. *et al.* Prolonged contact with dendritic cells turns lymph node-resident NK
656 cells into anti-tumor effectors. *EMBO Mol Med* **8**, 1039-1051, (2016).
657 40 Giavazzi, R., Alessandri, G., Spreafico, F., Garattini, S. & Mantovani, A. Metastasizing
658 capacity of tumour cells from spontaneous metastases of transplanted murine tumours. *Br J*
659 *Cancer* **42**, 462-472, (1980).
660 41 Wagner, M., Jonjic, S., Koszinowski, U. H. & Messerle, M. Systematic excision of vector
661 sequences from the BAC-cloned herpesvirus genome during virus reconstitution. *J Virol* **73**,
662 7056-7060, (1999).
663 42 Jonjic, S., Pavic, I., Lucin, P., Rukavina, D. & Koszinowski, U. H. Efficacious control of
664 cytomegalovirus infection after long-term depletion of CD8+ T lymphocytes. *J Virol* **64**,
665 5457-5464, (1990).
666 43 Reddehase, M. J. *et al.* Interstitial murine cytomegalovirus pneumonia after irradiation:
667 characterization of cells that limit viral replication during established infection of the lungs.
668 *J Virol* **55**, 264-273, (1985).
669
670

671 **Extended Data, Figures**

672

673 **Extended Data Figure 1. Expression of IL-1R8 in human and murine NK cells**

674 (a, b) IL-1R8 mRNA (a) expression in human primary NK cells, compared with T and B cells,

675 neutrophils, monocytes and *in vitro*-derived macrophages (a) and in human primary NK cell

676 maturation stages ($CD56^{br}CD16^{-}$, $CD56^{br}CD16^{+}$, $CD56^{dim}CD16^{+}$), and in the $CD56^{dim}CD16^{-}$ subset

677 (b).

678 (c) Representative FACS plot of human NK cell subsets and histograms of IL-1R8 expression in

679 NK cell subsets.

680 (d) IL-1R8 protein expression in human bone marrow precursors and mature cells.

681 (e) IL-1 receptor family members (Il1r1, Il1r2, Il1r3, Il1r4, Il1r5, Il1r6, Il1r8) mRNA expression in

682 murine primary NK cells isolated from the spleen.

683 (f) IL-1R8 protein expression in murine NK cells by confocal microscopy. Magnification bar:

684 10μm.

685 (g) Representative FACS plot of murine NK cell subsets.

686

687 (a, b, d) *p < 0.05, **p < 0.01, ***p < 0.001 One-way ANOVA. Mean ± SEM.

688 a, n=6 (NK and B cells) or n=4 donors; b, n=5 donors; d, n=4 donors; e, n=2 mice; f, representative

689 images out of four collected per group.

690 a, b, d, e, f, one experiment performed.

691

692 **Extended Data Figure 2. Phenotypic analysis of *Il1r8*$^{-/-}$ NK cells.**

693 (a, b) Representative FACS plot of murine NK cell subsets in *Il1r8*$^{+/+}$ and *Il1r8*$^{-/-}$ mice (a) and

694 histograms of KLRG1 expression in NK cells.

695 (c, d) NK absolute number and NK cell subsets (DN, CD11b^{low}, DP and CD27^{low}) in bone marrow,

696 spleen and blood of *Il1r8*$^{+/+}$ and *Il1r8*$^{-/-}$ newborn mice at 2 (c) and 3 (d) weeks of age.

697 (e) Frequency of bone marrow precursors in *Il1r8*$^{+/+}$ and *Il1r8*$^{-/-}$ mice.

698 (f) NKG2D, DNAM-1 and LY49H expression in peripheral NK cells and NK cell subsets of

699 *Il1r8*$^{+/+}$ and *Il1r8*$^{-/-}$ mice.

700 (g) Frequency of splenic Perforin^{+} NK cell subsets upon stimulation in *Il1r8*$^{+/+}$ and *Il1r8*$^{-/-}$ mice.

701 (h and i) Peripheral NK cell absolute number (h) and CD27^{low} NK cell frequency (i) in bone

702 marrow chimeric mice upon reconstitution (9 weeks).

703 (j and k) Peripheral NK cell (j) and NK cell subset (k) frequency in competitive chimeric mice

704 transplanted with 50% of *Il1r8*$^{+/+}$ CD45.1 cells and 50% of *Il1r8*$^{-/-}$ CD45.2 cells upon reconstitution

705 (9 weeks). Upon reconstitution a defective engraftment (12% instead of 50% engraftment) of *Il1r8*$^{-/-}$

706 stem cells was observed in competitive conditions.

707 (l) IFNγ production by *Il1r8*$^{+/+}$ and *Il1r8*$^{-/-}$ NK cells upon co-culture with LPS- or CpG-primed

708 *Il1r8*$^{+/+}$ and *Il1r8*$^{-/-}$ DCs.

709 (c-l) *$p < 0.05$, **$p < 0.01$, ***$p < 0.001$ between selected relevant comparisons, two-tailed

710 unpaired Student's t test. Centre values and error bars represent mean ± SEM. At least 5 animals per

711 group were used. c, d: 3 pooled experiments. e-l: one experiment was performed.

712

713 **Extended Data Figure 3. Mechanism of IL-1R8-dependent regulation of NK cells**

714 (a) Splenic CD27^{low} NK cell frequency in wild type, *Il1r8*$^{-/-}$, *Il18*$^{-/-}$, and *Il18*$^{-/-}$/*Il1r8*$^{-/-}$ mice.

715 (b) Peripheral CD27^{low} NK cell frequency in *wild-type*, *Il1r8*$^{-/-}$*, Il1r1*$^{-/-}$ and *Il1r8*$^{-/-}$*Il1r1*$^{-/-}$ mice (left)

716 and IFNγ production by splenic NK cells after IL-12 and IL-1β or IL-18 stimulation (right).

717 (c, d) Splenic CD27^{low} NK cell frequency in *Il1r8*$^{+/+}$ and *Il1r8*$^{-/-}$ mice upon commensal flora

718 depletion (c) and breeding in co-housing conditions (d).

719 (e) STED microscopy of human NK cells stimulated with IL-18. Magnification bar: 2μm.

720 (a-d) *p < 0.05, **p < 0.01, ***p < 0.001 between selected relevant comparisons, two-tailed

721 unpaired Student's t test; Centre values and error bars represent mean ± SEM. a, n= 3, 5, or 6 mice;

722 at least 5 animals per group were used (b-d). a-d: one experiment was performed. e: representative

723 images out of three collected from two donors.

724

725 **Extended Data Figure 4. RNA-seq analysis of *Il1r8*$^{+/+}$ and *Il1r8*$^{-/-}$ NK cells.**

726 (a) Metascape analysis of enriched gene pathways of resting and IL-18-activated *Il1r8*$^{+/+}$ and *Il1r8*$^{-/-}$

727 NK cells.

728 See also Supplementary Table 1 and data deposited in NCBI Gene Expression Omnibus accessible

729 through GEO Series accession number GSEXXXXX.

730

731 **Extended Data Figure 5. NK cell-mediated resistance to HCC and metastasis in IL-1R8-**

732 **deficient mice.**

733 (a) Macroscopic score of liver lesions in female *Il1r8*$^{+/+}$ and *Il1r8*$^{-/-}$ mice 6, 10 and 12 months after

734 DEN injection.

735 (b) HCC incidence in *Il1r8*$^{+/+}$ and *Il1r8*$^{-/-}$ female and male mice.

736 (c) Frequency of IFNγ^{+} NK cells in spleen of *Il1r8*$^{+/+}$ and *Il1r8*$^{-/-}$ tumor bearing mice.

737 (d) Macroscopic score of liver lesions in female *Il1r8*$^{+/+}$ and *Il1r8*$^{-/-}$ mice upon NK cell depletion.

738 (e) 2-DG quantification in lungs of *Il1r8*$^{+/+}$ and *Il1r8*$^{-/-}$ tumor bearing mice upon NK cell depletion.

739 (f) Primary tumor growth in *Il1r8*$^{+/+}$ and *Il1r8*$^{-/-}$ mice (25 days after MN/MCA1 cell line injection).

740 (g) Number of lung metastasis in *Il1r8*$^{+/+}$ and *Il1r8*$^{-/-}$ MN/MCA1 sarcoma bearing mice upon IFNγ

741 or IL-18 neutralization.

742 (h) Volume of lung metastases in *Il1r8*$^{+/+}$ and *Il1r8*$^{-/-}$ MN/MCA1-bearing mice upon depletion of

743 IL-17A or CD4^{+}/CD8^{+} cells.

744 (i) Number of lung metastases in *Il1r8*$^{+/+}$ and *Il1r8*$^{-/-}$, *Il1r1*$^{-/-}$, *Il1r1*$^{-/-}$/*Il1r8*$^{-/-}$ MN/MCA1-bearing

745 mice.

746 (j) Number of liver metastasis in *Il1r8*$^{+/+}$, *Il1r8*$^{-/-}$, *Il18*$^{-/-}$, *Il18*$^{-/-}$*Il1r8*$^{-/-}$ MC38 colon carcinoma

747 bearing mice.

748 (k) *Il1r8*$^{+/+}$ and *Il1r8*$^{-/-}$ NK cell absolute number three or 7 days after adoptive transfer.

749 (l) *In vivo* *Il1r8*$^{+/+}$ and *Il1r8*$^{-/-}$ NK cell proliferation three days after adoptive transfer.

750 (m) *Ex vivo* IFNγ production and degranulation upon 4-hour stimulation with PMA-Ionomycin, IL-

751 12 and IL-18 in adoptively transferred *Il1r8*$^{+/+}$ and *Il1r8*$^{-/-}$ NK cells.

752 (n) Volume of lung metastasis of *Il1r8*$^{+/+}$ MN/MCA1 sarcoma bearing mice after adoptive transfer

753 of *Il1r8*$^{+/+}$ and *Il1r8*$^{-/-}$ NK cells.

754 (a, c-e, g-j, m-n) *p < 0.05, **p < 0.01, ***p < 0.001 between selected relevant comparisons, two-

755 tailed unpaired Student's t test or Mann-Whitney test. #p<0.05, ##p<0.01, Kruskal-Wallis and

756 Dunn's multiple comparison test. Centre values and error bars represent mean ± SEM. a, n=9, 10,

757 11, 18, 21 mice; b, n=8-21 mice; c, n=6 mice; d, n= 10, 12, 13 mice; e, n=4 (*Il1r8*$^{-/-}$ isotype) or n=5;

758 f, n=10; g, n=6, 7, 9, 10 mice; h, n=5, 6, 12 mice; i, n=6, 8, 10 mice; j, n=4, 5, 7 mice; k, l, m, n=3

759 mice; n, n=9, 10, 12 mice. Representative experiment out of 3 (a, b), 2 (d), 6 (f), or one (c, e, g-n)

760 experiment performed.

761

762 **Extended Data Figure 6. NK cell-mediated antiviral resistance in IL-1R8-deficient mice**

763 (a) Cytokine serum levels in *Il1r8*$^{+/+}$ and *Il1r8*$^{-/-}$ infected mice (1.5 and 4.5 days post infection).

764 $^{*}p < 0.05$, $^{**}p < 0.01$, $^{***}p < 0.001$, unpaired Student's t test. Centre values and error bars

765 represent mean ± SEM. n=5 mice. One experiment was performed.

766

767 **Extended Data, Table**

768 **Table 1 - Serum cytokine and liver enzyme levels in HCC-bearing mice.**

769 *: Samples with not detectable levels were not included in the analysis.

770 **: levels are U/L.

771 ***: n=5, 8 months after DEN

772

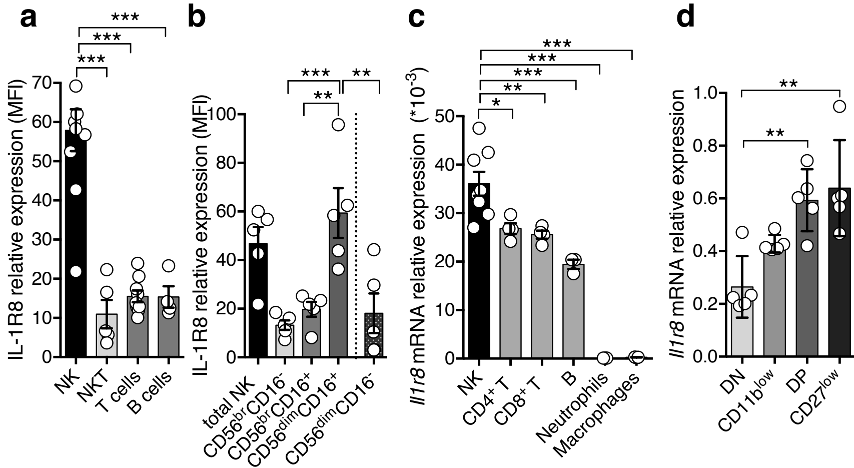
a
b
c
d
IL-1R8 relative expression (MFI)
NK
NKT
T cells
B cells
total NK
CD56brCD16-
CD56brCD16+
CD56dimCD16+
CD56dimCD16-
Il1r8 mRNA relative expression (*10-3)
CD4+ T
CD8+ T
B
Neutrophils
Macrophages
Il1r8 mRNA relative expression
DN
CD11blow
DP
CD27low
***
**
*

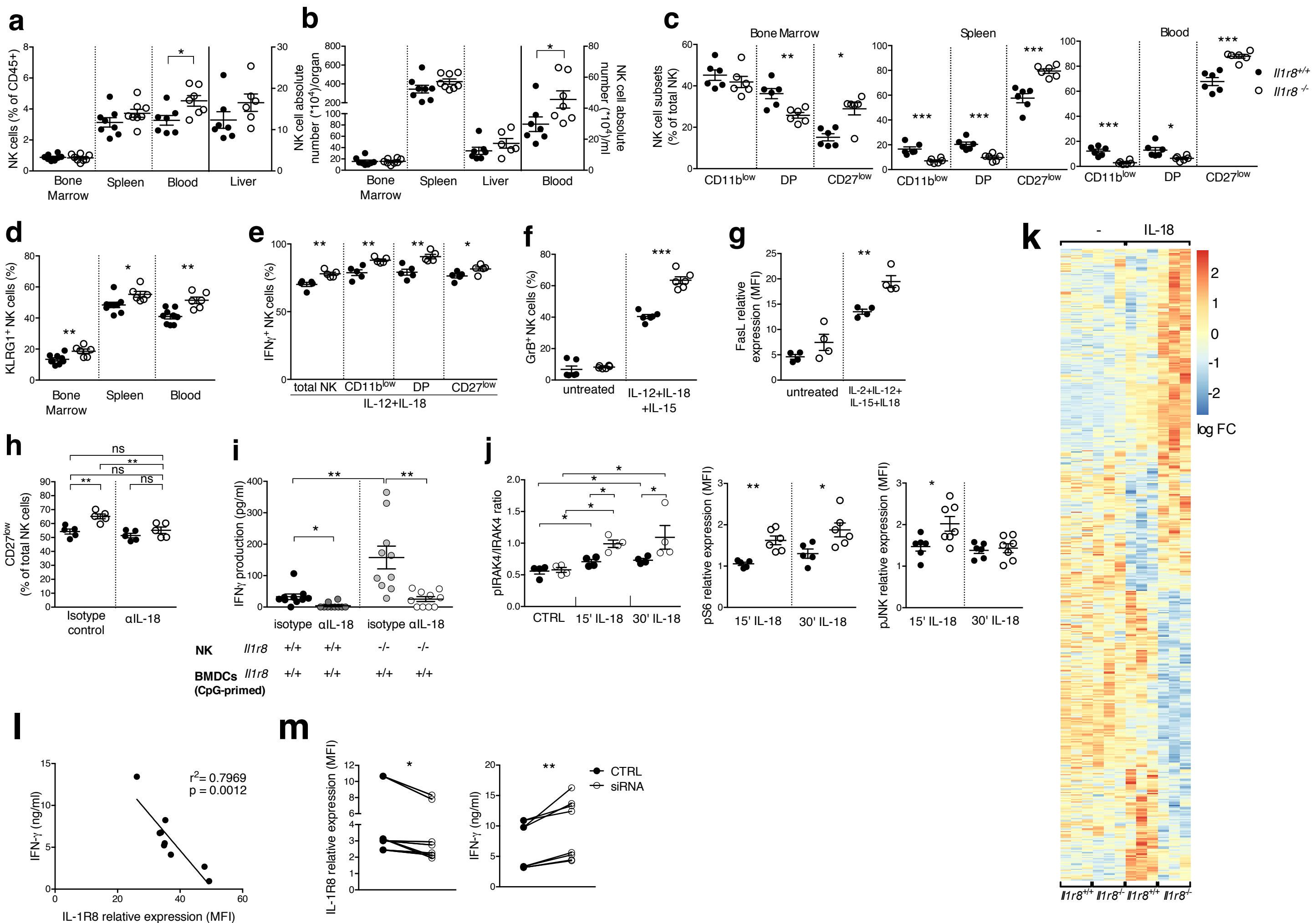

a
NK cells (% of CD45+)
Bone Marrow
Spleen
Blood
Liver
b
NK cell absolute number (*10⁴)/organ
NK cell absolute number (*10⁴)/ml
Bone Marrow
Spleen
Liver
Blood
c
Bone Marrow
Spleen
Blood
NK cell subsets (% of total NK)
CD11b^low
DP
CD27^low
Il1r8+/+
Il1r8-/-
d
KLRG1+ NK cells (%)
Bone Marrow
Spleen
Blood
e
IFNγ+ NK cells (%)
total NK
CD11b^low
DP
CD27^low
IL-12+IL-18
f
GrB+ NK cells (%)
untreated
IL-12+IL-18 +IL-15
g
FasL relative expression (MFI)
untreated
IL-2+IL-12+ IL-15+IL18
k
-
IL-18
log FC
Il1r8+/+
Il1r8-/-
Il1r8+/+
Il1r8-/-
h
CD27low (% of total NK cells)
ns
**
ns
ns
Isotype control
αIL-18
i
IFNγ production (pg/ml)
isotype
αIL-18
isotype
αIL-18
NK Il1r8 +/+ +/+ -/- -/-
BMDCs (CpG-primed) Il1r8 +/+ +/+ +/+ +/+
j
pIRAK4/IRAK4 ratio
CTRL
15' IL-18
30' IL-18
pS6 relative expression (MFI)
15' IL-18
30' IL-18
pJNK relative expression (MFI)
15' IL-18
30' IL-18
l
IFN-γ (ng/ml)
IL-1R8 relative expression (MFI)
r²= 0.7969
p = 0.0012
m
IL-1R8 relative expression (MFI)
IFN-γ (ng/ml)
CTRL
siRNA

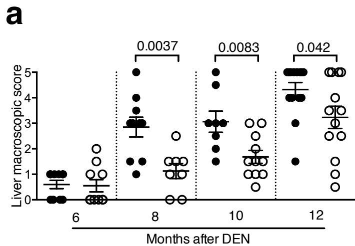
a
Liver macroscopic score
0.0037
0.0083
0.042
6
8
10
12
Months after DEN
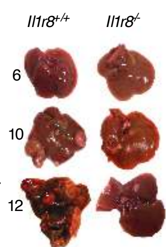
Il1r8+/+
Il1r8-/-
6
10
12
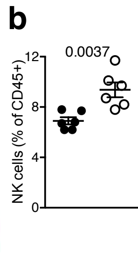
b
NK cells (% of CD45+)
0.0037
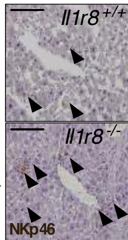
Il1r8 +/+
Il1r8 -/-
NKp46
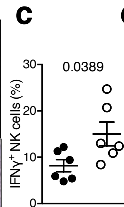
c
IFNγ+ NK cells (%)
0.0389
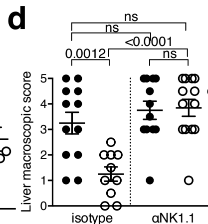
d
ns
ns
<0.0001
0.0012
ns
Liver macroscopic score
isotype
αNK1.1
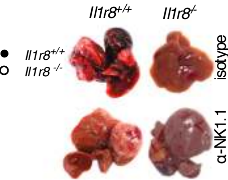
Il1r8+/+
Il1r8-/-
isotype
α-NK1.1
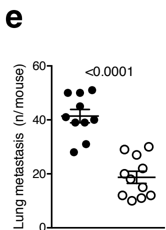
e
Lung metastasis (n/ mouse)
<0.0001
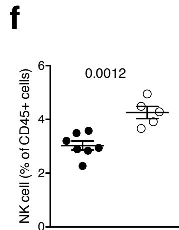
f
NK cell (% of CD45+ cells)
0.0012
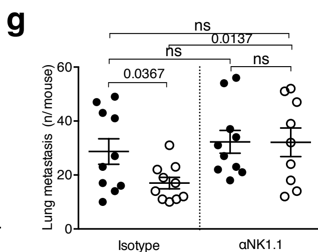
g
ns
0.0137
ns
ns
0.0367
Lung metastasis (n/ mouse)
Isotype
αNK1.1
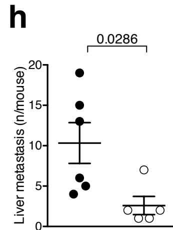
h
0.0286
Liver metastasis (n/mouse)
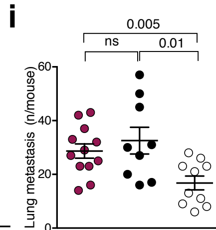
i
0.005
ns
0.01
Lung metastasis (n/mouse)
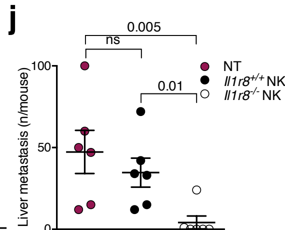
j
0.005
ns
0.01
Liver metastasis (n/mouse)
NT
Il1r8+/+ NK
Il1r8-/- NK

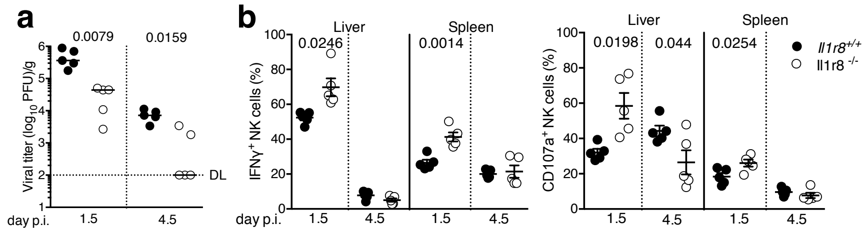

c
Liver
0.0004
0.0004
0.0188
Spleen
0.0076
ns
Lung
0.0176
ns
Brain
0.0154
0.01
Viral titer (log_{10} PFU)/g
DL
NT
Il1r8+/+ NK
Il1r8-/- NK

d
0.0039
0.005
IFNγ+ cells (% of NK1.1+ CD3- cells)
NK cells
ILC1